Supersonic Bi-Directional Flying Wing Configuration with Low Sonic Boom and High Aerodynamic Efficiency

Clemence Berger *, Kevin Carmona †, Daniel Espinal ‡, Hong-Sik IM §, Ge-Cheng Zha ¶

Dept. of Mechanical and Aerospace Engineering

University of Miami

Coral Gables, Florida 33124

E-mail: gzha@miami.edu

Abstract

In this paper, a parametric study is conducted to optimize a business jet using supersonic bi-directional (SBiDir) flying wing (FW)aiming at achieving high aerodynamic efficiency and low sonic boom. The SBiDir-FW concept has a symmetric planform about both longitudinal and span axes, allowing the plane to achieve high efficiency at both supersonic and subsonic by rotating by 90° in flight. With this parametric study, the L/Dp achieves 15 at M=1.6, 16 at M=2.0, whereas the sonic boom remains smooth without N-wave. The smooth peak over pressure value is 0.3 psf at M=1.6, 0.4 psf at M=2.0. It indicates that the conventional N-wave could be replaced by a strong acoustic wave, which generates a much less impulsive force and hence noise. The supersonic aspect ratio of the present configuration is 0.33 and the subsonic aspect ratio is 33, which ensures high performance at both supersonic and subsonic. The study shows that the sharp and long nose configuration with ultra-slender body is favorable to both high aerodynamic efficiency and low sonic boom. The numerical results demonstrate that the SbiDir-FW could be a very promising concept for supersonic flight. Further improvement can still be made by using systematic automated design optimization.

1   Introduction

Supersonic commercial flight has always been of great interest, due to its potential to reduce inter-continental travel time. However efforts to make supersonic commercial flight both economically and environmentally viable have yet to be made.

Supersonic transports have two major problems: efficiency and noise. Efficiency is first affected by the wave drag due to the strong shock waved created during supersonic flight. The second factor that affects efficiency is the large flight speed disparity between take-off/landing and cruise. In fact, for any airplane configuration at take-off and landing, the low flight speed favors a high aspect ratio and low wing sweep angle. High-speed supersonic cruise however requires the opposite characteristics. For a conventional wing-tube configuration, a compromise between low speed take-off/landing and high-speed cruise efficiency is required. As for the noise issue, it is caused by the sonic boom that propagates to ground from the shock waves created by a supersonic airplane and its components. Plotkin and Maglieri [1] gave an overview of the sonic boom research on the state of the art and the problems that need to be solved.

The flying wing concept that avoids the conventional tube fuselage and wing can result in improved aerodynamic efficiency during a supersonic flight. However the use of a supersonic flying wing for civil

---

*   Visiting Graduate Student, ENSMA
†   Visiting Graduate Student, ENSMA
‡   PhD Student, University of Miami
§   PhD Student, University of Miami
¶   Associate Professor, Director of CFD and Aerodynamics Lab, University of Miami

transport has rarely been studied. Jones' concept of a supersonic oblique flying wing (OFW)[2] brings an advantage: the sweep angle can be varied during the flight mission. It hence can obtain a high aspect ratio at low speed and a low aspect ratio at high speed [3, 4]. However the asymmetric configuration of OFW about the flight direction can create some difficulties. First it creates some problems concerning stability and control [5, 6]. Second, in order to comfortably accommodate the passengers with enough overhead space, the airfoil needs to be thick and it creates large wave drag. Nevertheless this configuration, even though it might increase the aerodynamic efficiency, does not take into account the problem of sonic boom, which is a major problem to make a supersonic commercial flight environmentally viable.

To minimize sonic boom, there are in general two strategies: The first strategy is to implement nose bluntness following the area rule suggested by Jones, Seebass, and George [7, 8, 9, 10]. A blunt nose design creates a shock distribution in which the greatest shock strengths are near the aircraft and the shocks are weakened gradually due to interaction with expansion waves as the shock waves travel from the aircraft to the ground. Unfortunately, this design also induces substantial wave drag since the entropy increase due to the strong shock waves is irreversible. The second strategy is to use a sharp nose in order to generate weak shock or isentropic compression to minimize or cancel shock waves and sonic boom. The sharp nose strategy is aerodynamically efficient but may produce a strong shock at mid-field and far-field distances from the aircraft. The Gulfstream Quiet Spike TM is an example using a sharp nose spike to reduce sonic boom [11]. However, the long and thin spike of Gulfstream Quiet Spike TM may create some structure stability problems. In principle, a sharp nose with isentropic compression is more likely to achieve both high aerodynamic efficiency and low sonic boom than the nose bluntness method.

Zha recently suggested a novel concept of supersonic bi-directional flying wing (SBiDir-FW) aimed at achieving high aerodynamic efficiency at both supersonic and subsonic, and reduce sonic boom at the same time [12, 13, 14]. The SBiDir-FW will rotate 90° between subsonic and supersonic mode to achieve high aerodynamic performance for both subsonic and supersonic. The ultra-slender supersonic configuration and isentropic compression pressure surface will reduce the sonic boom and replace the conventional N-wave by a smooth wave. As the first numerical simulation effort in [14] with Mach number of 1.6, Zha et al achieved a smooth ground sonic boom signature with the peak value of 0.3psf at zero angle of attack, which is very encouraging not just because of the low over pressure, but also because the conventional N-shape shock wave is removed. However, the L/Dp of 5.3 achieved at zero angle of attack is not outstanding. In [15], Espinal et al conduct a preliminary design using SbiDir-FW for a supersonic civil transport.

The purpose of this paper is to perform a parametric study to improve L/D of SBiDir-FW while maintaining the smooth sonic boom signature and low over pressure value. Even though the propulsion system is not included in the simulation, the high L/Dp and smooth and low sonic boom indicate that the SBiDir-FW is a very promising concept for supersonic flight.

2 The SBIDIR-FW Concept

The fundamental concept of SBiDir-FW consists of a flying wing or blended wing-body configuration with a symmetric planform about both the longitudinal and span axes with two flight directions altered by 90°. For supersonic flight, the planform will rotate 90° from the subsonic mode.

The subsonic aspect ratio will be increased by $(\frac{L}{b})^2$, where L is the airplane length and b its span:

$$AR_{M<1} = ((\frac{L}{b})^2) * AR_{M>1}$$

Fig. 1 shows the subsonic flight mode with high aspect ratio and Fig. 2 shows the supersonic flight with a very low aspect ratio after rotation 90°. Moreover, the sweep angle at subsonic will be largely reduced :

$$\delta_{M<1} = 90^o - \delta_{M>1}$$

Another characteristic that will help achieve high aerodynamic efficiency at both subsonic and supersonic speed is the thickness of the airfoil. Because a thin airfoil is preferred for supersonic flight, the circular-arc airfoil was designed to have a thickness equal to 3% of the local chord length. This 3% thickness was kept

constant for the supersonic configuration throughout the span. Due to the fact that the span is significantly shorter than the length in the subsonic flight direction, the thickness is significantly increased at subsonic mode, as highlighted in Fig. 3, therefore bringing the flying wing to achieve high lift coefficient at subsonic. Fig.4 shows the supersonic mode after 90° rotation from the subsonic mode with the thin supersonic airfoil highlighted.

The symmetric planform will let the trailing edge become leading edge during the rotation and generate lift to stabilize the mode transition similar to a flying Frisbee. The desirable transition mode Mach number is high subsonic such as about 0.8 to avoid the unsteady force introduced by shock waves at supersonic. The yaw moment to rotate the airframe will be generated by ailerons or flaps on the two sides of the flying wing. This concept therefore does not require a power driven system to rotate, not adding a weight penalty nor a system complication to the design. With this concept of rotating a symmetric flying wing, the conflict between supersonic and subsonic aerodynamic performance for a conventional tube-wing configuration is hence removed. High subsonic performance will be translated to high supersonic performance as the planform rotates.

The other important purpose of SBiDir-FW is to reduce downward shock and therefore sonic boom by using a sharp nose and an isentropic compression pressure surface. At $AoA = 0$, the flat pressure surface of the airplane will cancel the shock responsible for sonic boom propagated to the ground [14]. However, the L/D is not high enough at AoA =0°. This paper is to seek higher L/D at higher AoA while maintain the low sonic boom with smooth ground signature.

3 Flight Mission

The flight mission is a 10 passenger business jet with range of 4000 nm at altitude of 60,000 ft. The full length of the plane is 78m at supersonic. However in order to decrease the space due to the wing span at take off and landing, the tip part of the wings will be retracted in subsonic mode. The passenger weight including baggage is assumed to be 250 lbs per passenger for a total payload of 2.5 Klb. The estimated fuel weight required for the mission is 3.8 Klb.

4 CFD Model Validation

The in house FASIP(Flow Acoustics Structural Interaction Package) CFD code is used for the simulation. FASIP has been intensively validated for various 2D and 3D steady and unsteady flows. FASIP has implemented advanced numerical algorithms including various approximate Riemman solvers [16, 17, 18], 3rd order MUSCL Schemes, high order WENO schemes and central differencing schemes [19, 20, 21, 22], non reflective boundary conditions [23],implicit unfactored Gauss-Seidel dual time stepping for unsteady calculation [24, 25], fluid structural interaction[26, 27, 28], RANS turbulence models[29, 30, 31], DES and LES [32, 33, 34, 35], preconditioning for incompressible flows[22], and high scalability parallel computing[36].

As the first step, it is necessary to validate our sonic boom simulation tools[14]. Simulation of sonic boom using CFD needs to emphasize on the off body phenomenon, which has different mesh requirement from predicting aerodynamic forces of an airplane[37]. The cone Model 1 in the NASA sonic boom wind tunnel testing [38] is used to validate the CFD mesh setup and numerical schemes selection. The half cone angle is 3.24°, the cone length is 2inch. The tested Mach number of 2.01 is calculated numerically for its near field sonic boom signature. The computed results are compared with the experiment [38] and the CFD results of Wintzer et al [39]. The far field sonic boom signature is extrapolated using the NASA NF Boom code [40] based on the method of Thomas [41]. The mesh is inclined at the Mach angle to resolve the oblique shock waves. The computational domain size is extended one chord upstream, two and a half chords above and below the cone, and four and half chords downstream of the cone. The inlet boundary conditions is to fix all the variables at the freestream conditions. The upper, lower, and downstream conditions are zero gradient extrapolation. As the initial trails, the RANS model with Baldwin-Lomax model was used and the near field sonic boom was significantly over-predicted due to the boundary layer thickness. The calculation is then switched to inviscid calculation as the methods used by other groups [37, 39, 42, 43]. For our CFD

solver, the inviscid calculation is conducted with Reynolds number set to 10^{16} in the Navier-Stokes solver and slip wall boundary conditions enforced. The predicted pressure signatures of the NASA cone Model 1 agree very well with the experiment and the numerical results of other research group[14].

5 Parametric Study

Mesh

The mesh used for a SBiDir-FW configuration is $161 \times 83 \times 61$ in the streamwise, radial and circumferential direction respectively as shown on Fig. 5. It is then divided in 16 blocks of $21 \times 83 \times 61$ for parallel computation. The mesh is inclined at the Mach angle to resolve the oblique shock waves. Our mesh will therefore be different when the Mach number of the study is changed. This dependency is shown on Fig. 6. Several boundary conditions are applied. The inlet boundary condition is set to fixed freestream conditions. Upper, lower and the side of the mesh are set with zero gradient interpolation. The plane is divided into 6 blocks which are set to wall boundary conditions. A symmetry boundary condition also has to be defined in order to create the results for the other half part of our design. Fig. 7 is the mesh refinement results and shows that the over pressure signature is not affected by mesh that has 1.5 more point in all the directions. It indicated that the over pressure signature computed using this mesh is converged. Fig. 8 shows the convergence history obtained with this mesh. It shows that the mean residual is decreased by 3 order of magnitude and the calculation is converged after 5000 iterations.

Results

The geometry model in [14] was composed of two sweep angles and one deflection location as shown on Fig. 9. The baseline configuration of the SBiDir-FW in [14] is composed of two sweep angles of 60° and 80° with the supersonic aspect ratio of 1 and subsonic aspect ratio of 7. In order to smoothen the profile and increase the control parameters of the configuration, the geometry model is modified to consist of 4 sweep angles and 3 axial deflection locations as shown in Fig. 10, which is a quarter of the whole geometry. The deflection is defined as the location percentage of the airplane half length and measured from the airplane leading edge.

The supersonic airfoil used to construct the flying wing is a simple circular arc and the airfoil thickness is 3%. The aspect ratio at supersonic is 0.33 and subsonic is 33.

The parametric study varies the sweep angles and deflection locations in order to find the configuration with the good aerodynamic performance and low sonic boom. In order to compare the efficiency of the different configurations tested, we introduce a measure of merit (MoM), taking into account the ratio of lift to drag, sonic boom and volume of the design, defined as below:

$$MoM = w_1 * (\frac{\frac{L}{D}}{\frac{L}{D}_{baseline}}) + w_2 * (\frac{1}{(\frac{dp}{dp_{baseline}})}) + w_3 * (\frac{V}{V_{baseline}})$$

where w_1, w_2 and w_3 are the equal weights with the value $\frac{1}{3}$, L is the lift, D the drag, dp the over-pressure, V the volume of the airplane. This MoM is to include the aerodynamic efficiency, sonic boom and aircraft volume in an equal manner. The higher the MoM, the more merit is the design. Tables 1 and 2 show the different MoM obtained for different sweep angles and deflection locations. Plots 11 and 12shows the values of L/D, dP_{max}, volume (normalized with baseline value)and MoM.

Design 1 to 20 use the configuration of 2 sweep angles. Design21 to 38 use the new parametric configuration with 4 sweep angles and 3 deflection locations. Design 38 achieves the best MoM. This parametric study shows that a thinner and longer nose will give a better sonic boom as reflected in Design 38. However the downstream sweep angle also has a very important role to play. In fact changing the downstream part will have a significant effect not only on the sonic boom as shown on Fig. 13 but also on the L/D ratio. On Fig. 13, all the configurations have the same 4 sweep angles and only the deflection point of the downstream part

are varied. For design 38, last deflection is located at 90% of the half length of the airplane, for design 39 it is of 80% and finally for design40, 75%. The L/D drops from 15.58 for design 38 to 15.06 for design39 to finally 14.63 for design40. The best configuration therefore appears to be a plane with a long nose and a very slender body. According to the MoM, Design38 is the highest merit configuration obtained in this parametric study with high L/D, low sonic boom, and high internal volume. The sweep angles used for this new design are 88°, 85°, 82° and 73°. The axis distances are 45%, 65% and 90% of half the total length. Both the results of Mach 1.6 and Mach 2 will be analyzed for Design 38.

Fig. 14 gives the value of lift and drag depending on the angle of attack at M=1.6 and M=2.0. Fig. 15 shows the lift to drag ratio of the airplane vs AoA at M=1.6 and 2.0 compared to the baseline. The results suggest that the aerodynamic efficiency of the SBiDir-FW Design38 reaches its peak at $AoA = 2$ at both Mach numbers. Moreover, it shows that at M=2.0, the lift to drag ratio rises up to 15.58 at AoA of 2° whereas it is of 15.08 at M=1.6. Compared to the baseline value of 11.32, Design 38 is therefore much more aerodynamically efficient than the initial SBiDir 80-60 design, and at the same time, the sonic boom is significantly lower.

The airplane configuration of Design38 has better aerodynamic efficiency at M=2.0 than at Mach=1.6. However, at Mach 2, the overpressure is higher than that at Mach 1.6 as shown in Fig. 16 for the two body length below the airplane. Nonetheless, compared to the baseline configuration, the dP is still very low even at Mach M=2.0.

Fig. 17 and 18 are the ground sonic boom at various angles of attack. This results were obtained by extrapolation using NASA NF Boom code [40] with a ground reflection factor of 1.9. At M=1.6, all AoA ground sonic boom signature preserves the smooth near field pressure shapes, whereas the baseline forms the N-wave with two shock waves pulses at higher than zero AoA [14]. However, at M=2.0 and AoA=4, the N-wave on the ground is formed. Fig. 19 is the ground sonic boom signature of M=1.6 and M=2.0 compared to the baseline at AoA=2. The baseline configuration achieves a smooth sonic boom signature at AoA=0 with the peak value of 0.3psf [14], but it has a typical N-wave shape at AoA=2 with the peak value of 1.1 psf.

The typical N-wave is a shock wave with two shock pulses whereas a smoothen curve is considered as an acoustic wave. Assuming the over-pressure wave sweeps across an infinitesimal fluid control volume , the impulsive force acting on the control volume would be:

$$\Delta F = \Delta m \cdot a \tag{1}$$

where, ΔF is the impulsive force, Δm is the mass flow of the control volume and a is the acceleration. Given that the acceleration a is the derivative from velocity V, Eq. 1 becomes:

$$\Delta F = \Delta m \cdot \frac{dV}{dt} \tag{2}$$

According to Euler's equation, $dp = -\rho V dV$, by replacing dV in Eq. 2 :

$$\Delta F = -\Delta m \frac{dp}{\rho V dV} \tag{3}$$

The mass flow rate can also be given as : $\Delta m = \rho V \Delta S$ where ΔS is the capture area of the control volume. Equation 3 thus becomes:

$$\Delta F = -\Delta S \frac{dp}{dt} = -\Delta S \frac{\Delta p}{\Delta t} \tag{4}$$

From equation 4, it is clear that ΔF depends on the pressure variation rate. For a N-wave shape, the Δt is an instant and is very small, the $\frac{\Delta P}{\Delta t}$ will thus be very large. The N-wave could hence create a significant impulsive force F. On the contrary, for the smooth wave, the pressure rise time is much longer and therefore diminishes the force induced by the overpressure wave tremendously. For an overpressure wave of same amplitude, a smooth wave will have a much smaller impulsive force. It means that the noise created by

the smooth wave will be much weaker than a N-wave with the same amplitude. Thus, obtaining a smooth ground overpressure signature is very important in order to achieve the lowest sonic boom possible.

Design38 achieves a smooth ground sonic boom signature at Mach number of 1.6 with the peak value of 0.3 psf at AoA=2 while the L/Dp is 15.06. At Mach 2, the over pressure peack is 0.4psf and the L/Dp is 15.58.Please note that the peak over-pressure value is from the smooth waves instead of the N-waves. This significant improvement of the low boom and high L/Dp is attributed to the low supersonic aspect ratio of 0.33 and high sweep angle. Such a low aspect ratio is beyond the limit of conventional supersonic planform design for take-off/landing performance. However, for SBiDir-FW configuration, the low supersonic aspect ratio of 0.33 is translated to high subsonic aspect ratio of 33, which will provide the airplane with high performance at both supersonic and subsonic.

Fig. 20 and 21 show the Mach number contours on the upper surface at respectively M=1.6 and M=2.0, which indicates a clear upward shock on the rear of the plane. It also shows the planform shape at $AoA = 2$, which presents a sharp, long nose and a very slender body. Fig. 22 and 23 show the mach number contour on the lower surface at M=1.6 and M=2.0, which indicate that the pressure is fairly uniform in most of the area.

Fig. 24 and 25 is the Mach number contours at 0%span (mid-plane). At the leading edge, the shock is mostly an acoustic wave at the angle of Mach cone. Interestingly, the front oblique shock has a slight concave shape and is very weak therefore minimizing wave drag. On the suction surface, a tail shock is formed at two third of the plane length. On the pressure surface, a shock is also formed at the same location mostly due to the propagation of the shock from the suction surface.

Fig. 26 and 27 is the surface isentropic Mach number distributions at 0%, 25%, 50% and 75% span against axial distance normalized by the local chord length. For both the Mach numbers, the distribution shapes are about the same. It can be seen that even though the absolute lift loading is highest at the mid-span plane, the loading coefficient is increased toward the outer span. The pressure distribution shape is similar to transonic condition due to the high sweep angle. The shock location is slightly downstream of the mid-chord location at the mid-span and is moved more downstream toward outer-span. The overall shock strength is not very strong with the peak Mach number of 1.35 at M=1.6 and 1.69 at M=2.0 due to the high sweep angle. The weak tail shock is beneficial to the low wave drag. Similar to the shock wave, the expansion wave also propagates to the pressure surface as shown by the rapid acceleration downstream of the mid-chord location.

In order to change the way the plane looks, and especially in effort to increase the volume of our design, a new kind of approach was considered as shown on Fig. 28. What is interesting with this kind of design is that one can have a very thin nose without loosing too much volume because the back of the plane has a high volume due to the sweep angles that are defined. The configuration presented is Design 47. The sweep angles used for this new design are 88°, 70°, 88° and 70°. The axis distances are 45%, 35%, and 10% of half the total length.

The aerodynamic characteristics of Design 47 compared with Design 38 at Mach 2 are given in table 3. It shows that the lift is decreased as well as the L/Dp, which goes down to 13.32. However Fig. ?? shows that the overpressure is lower than Design 38. The sonic boom on ground at Mach 2 is smooth and achieves a peak of 0.3psf at angle of attack 2. However what we can see is that even though the MoM suggests that Design 47 is better than Design 38, the volume , the main objective intended for improving is actually lower as shown in Table 3. Overall, this configuration indicates that there is a large room for overall improvement of MoM if a more intelligent and systematic optimization is utilized.

6   Conclusions

This paper conducts a parametric design study for an imaginary supersonic business jet based on supersonic bi-directional flying wing concept. The supersonic business jet is designed to have a payload of 10 passengers and range of 4000 nm to cruise at Mach 1.6 and 2.0 at altitude of 60,000 ft. The designed SbiDir-FW configuration provides a aspect ratio of 0.33 at supersonic and 33 at subsonic to achieve high aerodynamic performance at both supersonic and subsonic. The study indicates that a sharp and long nose configuration

with an ultra slender body is favorable to both aerodynamic performance and low sonic boom. The table below summarizes the results of the best design (Design 38) of the parametric study.

	Baseline	M=1.6	M=2.0
L/D	11.35	15.06	15.58
dP$_{2Lbelow}$	0.017	0.0037	0.0053
P$_{ground}$(psf)	1.1	0.3	0.4

Design 38 achieves a lift to drag ratio of 15 and 15.58 respectively at Mach 1.6 and Mach 2.0. Moreover this configuration maintains a smooth and low sonic boom of 0.3psf at Mach 1.6 and 0.4psf at M=2.0. It means that the conventional N-wave could be replaced by a strong acoustic wave, which is expected to generate a much less impulsive force and hence noise.

The SbiDir-FW concept appears to be a very promising concept for supersonic flight, achieving the very high aerodynamic efficiency and the low sonic boom needed in order to make it viable. More systematic research is however needed to optimize the configuration, in particular concerning the integration of the propulsion system.

7 Acknowledgment

References

[1] K. Plotkin, D. Maglieri, "Sonic Boom Research: History and Future," *AIAA*, pp. 2003–3575, 23,26 June 2003.

[2] R. Jones, "The Oblique Wing Aircraft Design for transonic and low supersonic speeds," *Acta Astronautica*, vol. 4, 1977.

[3] I. Desktop Aeronautics, "Oblique Flying Wings: An Introduction and White Paper." http://www.desktop.aero/library/whitepaper/index.html.

[4] M. Hirschberg, D. Hart, T. Beutner, "A Summary of a Half-Century of Oblique Wing Research," *AIAA*, p. 150, 2007.

[5] J.P Campbell, H.M Drake, "Investigation of Stability and Control Characteristics of an Airplane Model with a Skewed Wing in the Langley Free Flight Tunnel," *NACA TN-1208*, 1947.

[6] I.M Kroo, "The Aerodynamic Design of Oblique Wing Aircraft." Proceedings of the AIAA/AHS/ASEE Aircraft Systems Design and Technology Meeting, Washington D.C., 2005.

[7] L.B Jones, "Lower Bounds for Sonic Bangs," *Journal of the Royal Aeronautical Society*, vol. 65, pp. 433–436, 1961.

[8] R. Seebass, A. George, "Sonic-Boom Minimization," *Journal of the Royal Aeronautical Society of America*, vol. 51, pp. 686–694, 1972.

[9] R.J Mack, K.E Needleman, "A Methodology for Designing Aircraft to Low Sonic Boom Constraints," *NASA*, vol. TM-4246, 1991.

[10] D. Graham, "Quiet Supersonic Platform, Shaped Sonic Boom Demonstrator(SSBD) Program." FAA Civil Supersonic Aircraft Workshop, 2003.

[11] D.Howe, F.Simmons, D.Freund, "Development of the Gulfstream Quiet Spike TM for Sonic Boom Minimization," *AIAA paper*, vol. 2008-124, pp. 7–10, 2008.

[12] G.C Zha, "Supersonic Bi-Directionnal Flying Wing." Provisional patent application No.61172929, 27 Apr. 2009. Submitted to USPTO.

[13] G.C Zha, "Toward Zero Sonic-Boom and High Efficiency Supersonic UAS: A Novel Concept of Supersonic Bi-Directional Flying Wing." US Air Force Academic Outreach UAS Symposium, Grand Forks, ND, Aug. 4-6, 2009.

[14] G.C Zha, H. Im, D. Espinal, "Toward Zero Sonic Boom and High Efficiency Supersonic Flight, Part I: A Novel Concept of Supersonic Bi-Directional Flying Wing." AIAA paper 2010-1013, 48th AIAA Aerospace Sciences Meeting Including the New Horizons Forum and Aerospace Exposition, 4-7 January 2010, Orlando, Florida.

[15] D. Espinal, H. Im, B. Lee, J. Dominguez, H. Sposata, D. Kinard, G.C Zha, "Supersonic Bi-Directional Flying Wing, Part II: Conceptual Design of a High Speed Civil Transport." AIAA paper 2010-1393, 48th AIAA Aerospace Sciences Meeting Including the New Horizons Forum and Aerospace Exposition, 4 - 7 January 2010, Orlando, Florida.

[16] G.C.Zha, Y.Shen, B.Wang, "An Improved Low Diffusion E-CUSP Upwind Scheme," *Journal of Computer & Fluids*, vol. 48, pp. 214–220, 2011.

[17] G.C.Zha, "Low Diffusion Efficient Upwind Scheme," *AIAA Journal*, vol. 43, 2005.

[18] G.C.Zha, Z.J Hu, "Calculation of Transonic Internal Flows Using an Efficient High Resolution Upwind Scheme," *AIAA Journal*, vol. 42, No2, pp. 205–214, 2004.

[19] Y.Q Shen, G.C Zha, "Improvement of the WENO Scheme Smoothness Estimator," *International Journal for Numerical Methods in Fluids*, vol. DOI:10.10002/fld.2186, 2009.

[20] Y.Q Shen, G.C Zha, X.Y Chen, "High Order Conservative Differencing for Viscous Terms ans the Application to Vortex-Induced Vibration Flows," *Journal of Computational Physics*, vol. 228(2), pp. 8283–8300, 2009.

[21] Y.Q.Shen, G.C.Zha, B.Wang, "Improvement of Stability and Accuracy of Implicit WENO Scheme," *AIAA Journal*, vol. 47, pp. 331–344, 2009.

[22] Y.Q.Shen, G.C.Zha, "Improved Seventh-Order WENO Scheme." AIAA Paper 2010-1451, 48th AIAA Aerospace Sciences Meeting, Orlando,FL, 4-6 Jan. 2010.

[23] X.Chen, G.C.Zha, "Implicit Application of Non-Reflective Boundary Conditions for Navier-Stokes Equations in Generalized Coordinates," *International Journal for Numerical Methods in Fluids*, vol. 50, 2006.

[24] Z.J.Hu, G.C.Zha, "Calculation of 3D Compressible Using an Efficient Low Diffusion Upwind Scheme," *International Journal for Numerical Methods in Fluids*, vol. 47, pp. 253–269, 2004.

[25] Y.Q.Shen, G.C.Zha, "A Comparison Study of Gauss Seidel Iteration Methods for Internal and External Flow," *AIAA Paper*, vol. 4332, 2007.

[26] X.Y Chen, G.C.Zha, M.T.Yang, "Numerical Simulation of 3D Wing Flutter with fully Coupled Fluid-Structural Interaction," *Journal of Computers and Fluids*, vol. 36,No 5, pp. 856–867, 2007.

[27] X.Y Chen, G.C.Zha, "Fully Coupled Fluid-Structural Interaction Using an Efficient High Resolution Upwind Scheme," *Journal of Fluids and Structure*, vol. 20, pp. 1105–1125, 2007.

[28] B.Y Wang, G.C.Zha, M.T.Yang, "High Fidelity Simulation of Non Linear Fluid-Structural Interaction with Transonic Airfoil Limit Oscillations," *Journal of Fluids and Structures*, 2010.

[29] B.Y Wang, B.Haddoukessouni, J.Levy, G.C.Zha, "Numerical Investigations of Injection Slot Size Effect on the Performance of Co-Flow Jet Airfoil," *Journal of Aircraft*, 2008.

[30] B.Y Wang, G.C.Zha, "Comparison of a Low Diffusion Scheme E-CUSP and the Roe Scheme for RANS Calculation," *AIAA Paper*, 2008.

[31] P.Coronado, B.Y.Wang, G.C.Zha, "Delayed Detached Eddy Simulation of Shock Wave / Turbulent Boundary Layer Interactio," *AIAA Paper*, Jan.2010.

[32] X.Y Chen,B.Y. Wang G.C.Zha, "Detached Eddy Simulation of 3D Wing Flutter with Fully Coupled Fluid Structural Interaction," *AIAA Paper*, 2010.

[33] Y.Q Shen, G.C.Zha, "Comparison of High Order Schemes for Large Eddy Simulation of Circular Cylinder Flows," *AIAA/Submitted to Journal of Computational Physics*, 2009.

[34] B.Y. Wang, G.C.Zha, "Detached Eddy Simulations of a Circular Cylinder Using a Low Diffusion E-CUSP anf High Order WENO Scheme." AIAA Paper 2008-3855, 48th AIAA Fluid Dynamics Conference, June 23-26 2008.

[35] Y.Q Shen, G.C.Zha, "Simulation of Flows at All Speeds with WENO Scheme and Preconditionning." AIAA Paper 2009-1312, AIAA 47th Aerospace Science Meeting, Jan. 5-8 2009.

[36] B.-Y. Wang and G.-C. Zha, "A General Sub-Domain Boundary Mapping Procedure For Structured Grid CFD Parallel Computation," *AIAA Journal of Aerospace Computing, Information, and Communication*, vol. 5, No.11, pp. 2084–2091, 2008.

[37] J.H Casper, S.E Cliff, S.D Thomas, M.A Park, M.S McCullen, J.E Melton, D.A Durston, "Assessment of Near-Field Sonic Boom Simulation Tools." AIAA Paper 2008-6592, 26th AIAA Applied Aerodynamics Conference, Honolulu, Hawaii, 18-21, August 2008.

[38] H.W Carlson, R.J Mack and O.A Morris, "A Wind Tunnel Investigation of the Effect of Body Shape on Sonic Boom Pressure Distribution." NASA TN-D-3106, Nov.1965.

[39] M. Wintzer, M. Nemec, M.J Atmosis, "Adjoint-Based Adaptive Mesh Refinement for Sonic Boom Prediction." AIAA Paper 2008-6592, 26th AIAA Applied Aerodynamics Conference, Honolulu, Hawaii, 18-21, August 2008.

[40] D.A Durston, "Sonic Boom Extrapolation and Sound Level Prediction." Unpublished document, NASA Ames Research Center, Sept.2009.

[41] C.L Thomas, "Extrapolation of Sonic Boom Pressure Signatures by the Waveform Parameter Method." NASA TN-D-6832, June 1972.

[42] H. Ishikawa, Y. Makino, T. Ito and F. Kuroda, "Sonic Boom Prediction Using Multi-Block Structured Grids CFD Code Considering Jet-ON Effects," *AIAA*, vol. 3508, June 2009.

[43] S. Choi, J.J Alonso, I.M. Kroo and M. Wintzer, "Multi-Fidelity Design Optimization of Low Boom Supersonic Business Jets," *AIAA*, vol. 4371, 2004.

Design	Sweep1	Sweep2	Defl	MoM	Design	Sweep1	Sweep2	Defl (%)	MoM
1	80	60	25	1.00	**11**	80	60	20	1.01
2	75	60	25	1.07	**12**	80	60	15	1.05
3	70	60	25	1.15	**13**	80	60	40	1.26
4	87	60	25	0.832	**16**	80	70	30	1.25
5	80	65	25	1.07	**17**	80	75	35	1.48
6	80	55	25	0.904	**18**	70	70	25	1.29
7	80	70	25	1.18	**19**	75	75	25	1.35
8	80	75	25	1.34	**20**	80	80	25	1.61
9	80	60	30	1.03					
10	80	60	35	1.21					

Table 1: Definition and MoM of variation 1 to 20 with the model used in [14]
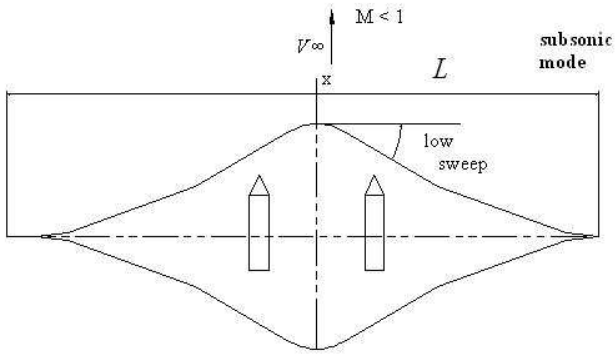
Figure 1: Sketch of a SBiDir-FW Planform flying in subsonic mode (not to scale)
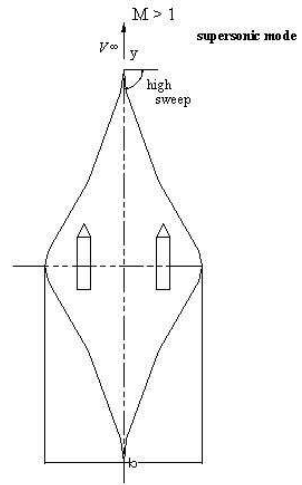
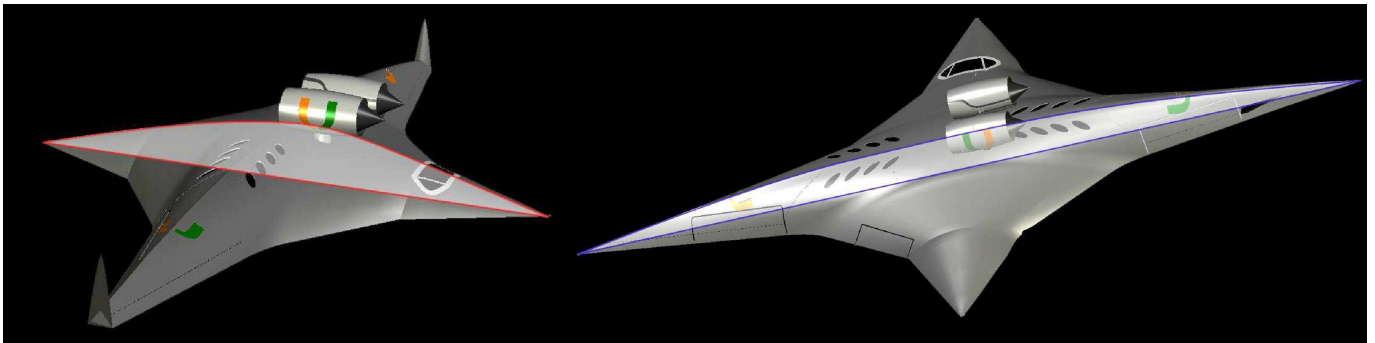Figure 2: Sketch of a SBiDir-FW Planform flying in supersonic mode (not to scale)

Figure 3: Subsonic mode
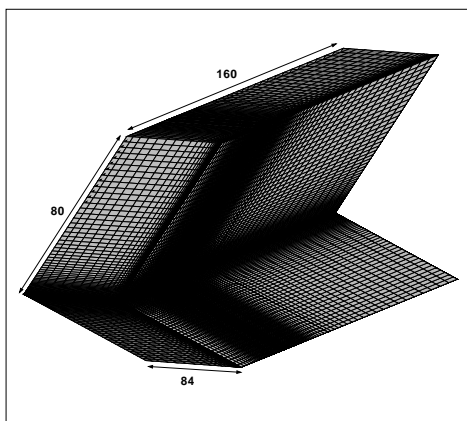

Figure 4: Supersonic mode

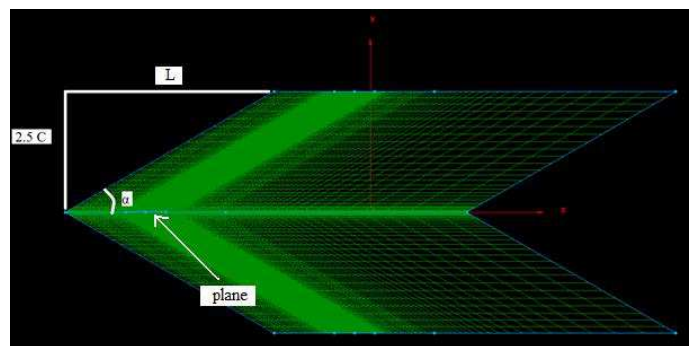Figure 5: 3D view of the SBiDir mesh with dimensions

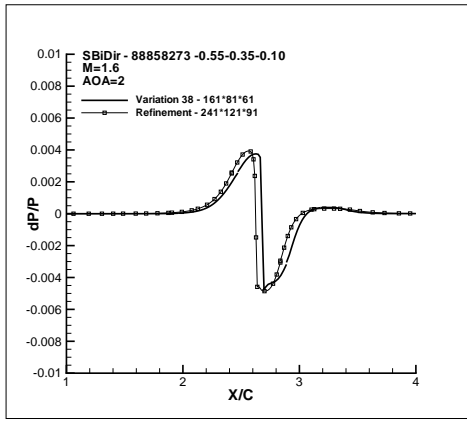Figure 6: Side view of the mesh with dependency to the mach angle

10

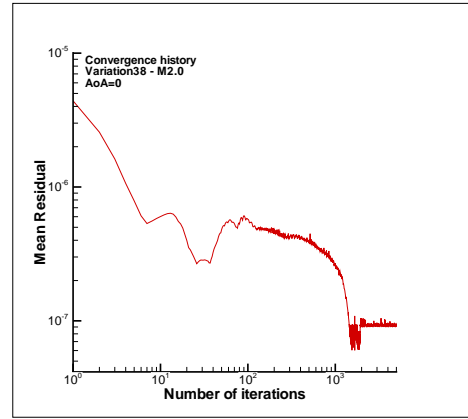Figure 7: Comparison of the computed over-pressure at two and a half body lengths below for mesh refinement study

Figure 8: Convergence history for Design 38 at M=2.0
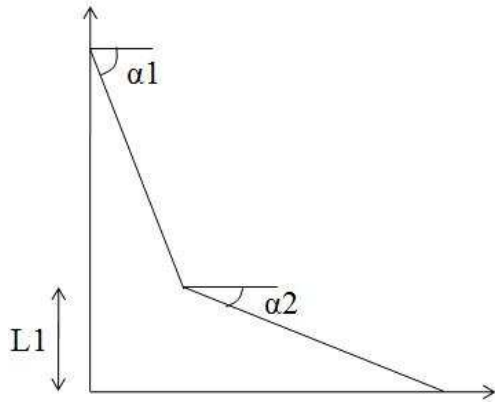
Figure 9: Former parametric definition of SbiDir-FW edge
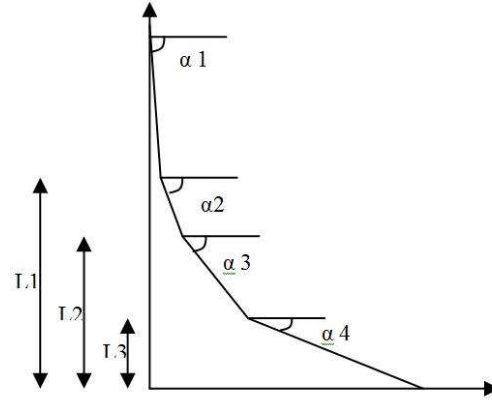
Figure 10: New parametric definition of SbiDir-FW edge

Design	Sweep1	Sweep2	Sweep3	Sweep4	Defl1	Defl2	Defl3	MoM
21	85	80	75	70	70	50	25	1.24
22	85	82	79	76	70	50	25	1.52
23	85	75	70	65	70	50	25	1.09
24	80	80	65	60	70	50	25	1.07
25	85	80	75	70	70	50	20	1.26
26	85	80	75	70	70	55	15	1.27
27	85	80	75	70	65	45	20	1.28
28	85	80	75	70	60	35	20	1.30
29	85	80	75	70	55	35	10	1.42
30	85	82	79	73	55	50	10	1.50
31	88	83	78	76	75	35	25	1.38
32	88	83	78	76	55	50	10	1.67
33	88	85	82	79	75	35	10	1.90
34	88	85	82	79	55	35	10	2.07
35	88	82	79	76	55	35	10	1.76
36	88	85	79	76	55	35	10	1.90
37	88	85	76	73	55	35	10	1.60
38	88	85	82	73	55	35	10	2.13

Table 2: Definition and MoM of variation 21 to 38 with the new geometry

11
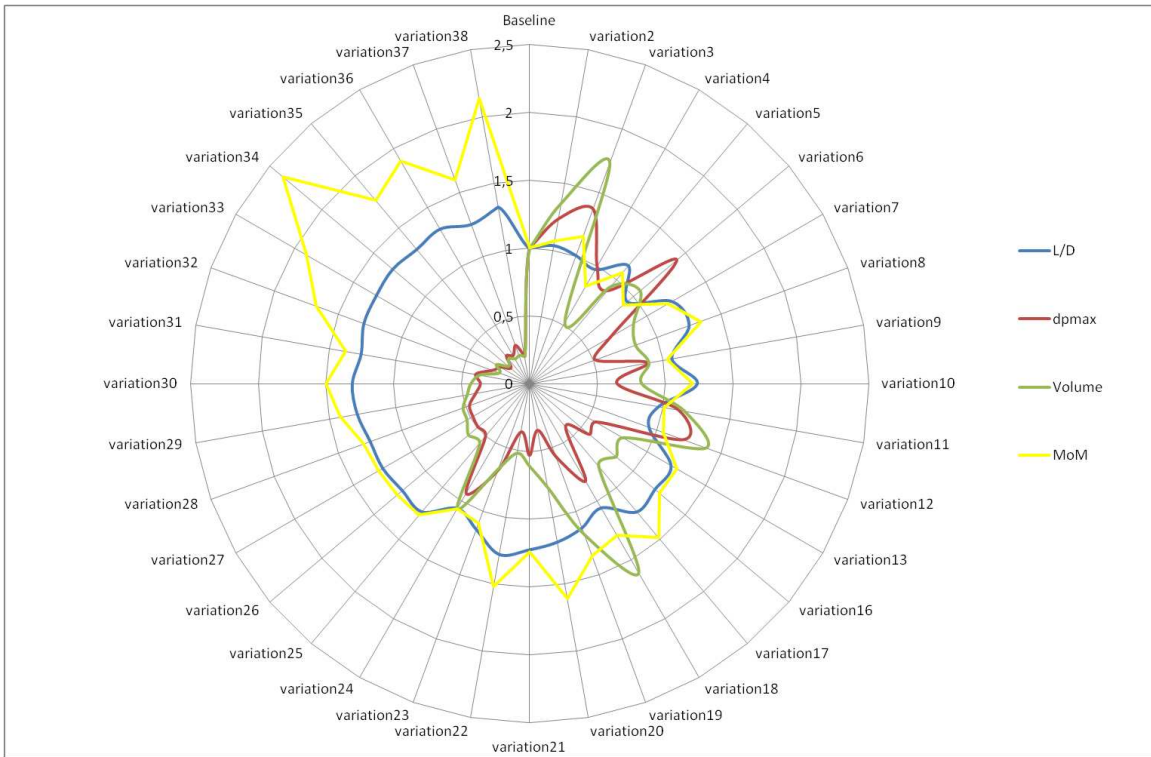
Figure 11: Values of L/D, dPmax, Volume and MoM for variations 1 to 38 at M=1.6
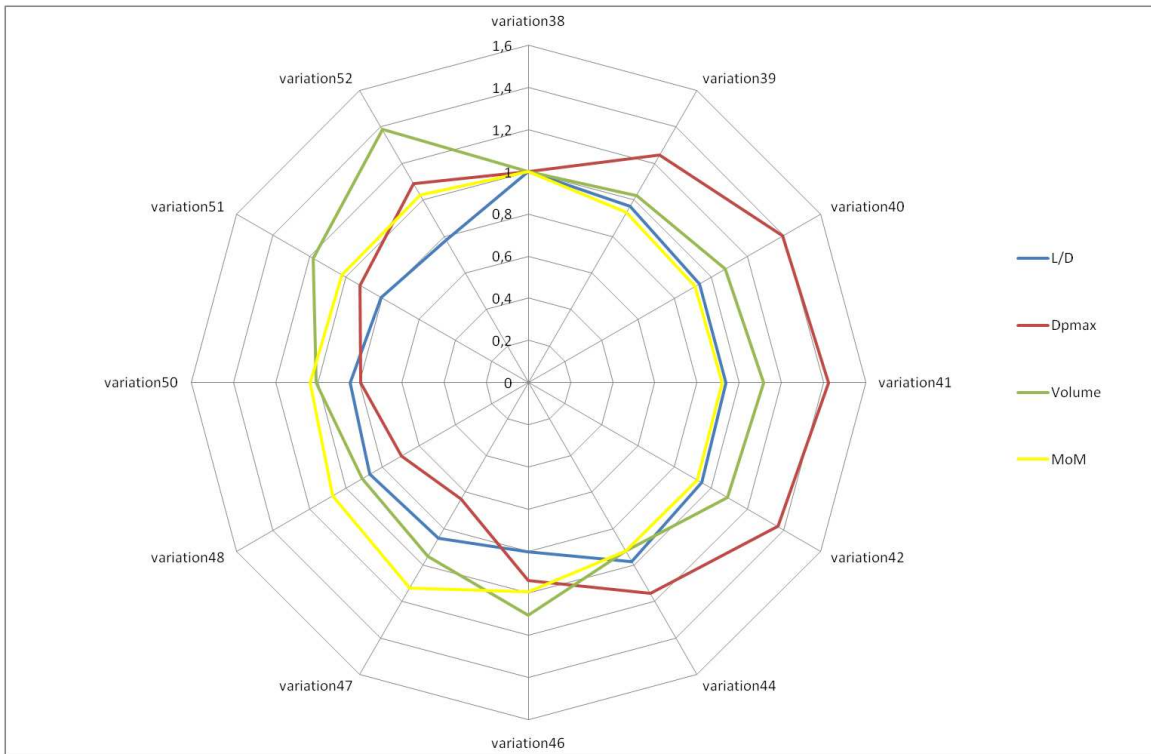
Figure 12: Values of L/D, dPmax, Volume and MoM for variations 38 to 52 at M=2.0
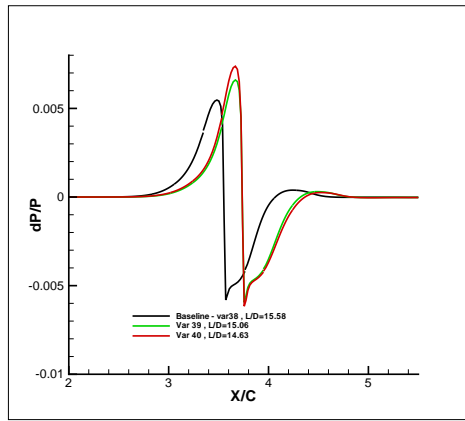
Figure 13: Computed overpressure two length below the aircraft for Design 38, 39 and 40
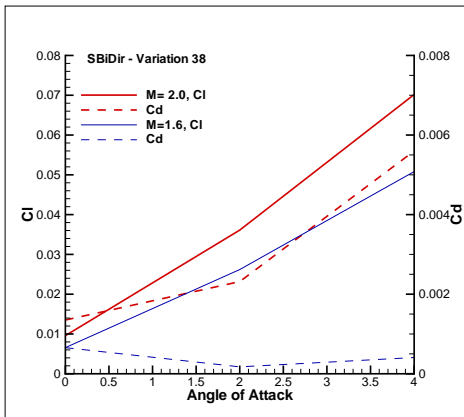
Figure 14: Lift and Drag coefficient vs AoA for Design38 at M=1.6 and M=2.0
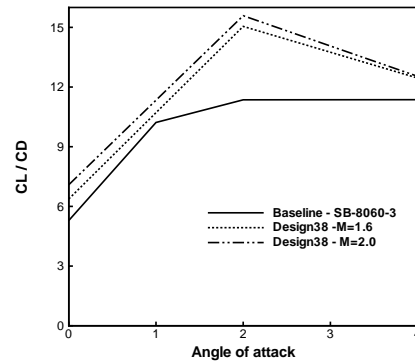
Figure 15: Lift over Drag ratio for the baseline and Design 38 at M=1.6 and M=2.0
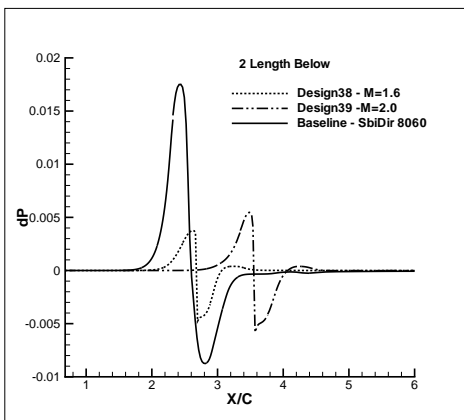
Figure 16: Computed pressure signature at two lengths below at AoA=2 for Design38 at M=1.6 and M=2.0 compared to the baseline
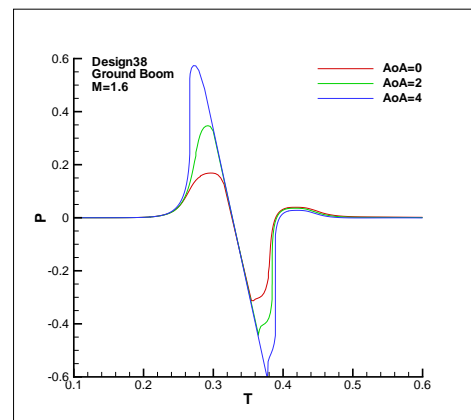
Figure 17: Computed pressure signature on the ground vs AoA for Design38 at M=1.6
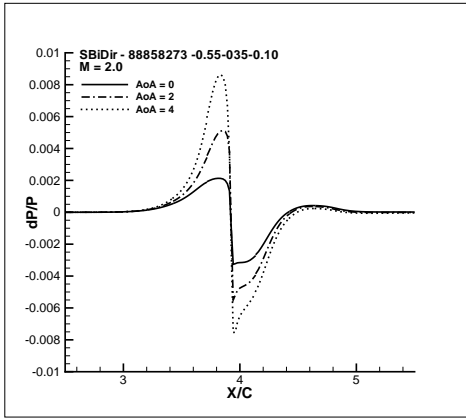
Figure 18: Computed pressure signature on the ground vs AoA for Design38 at M=2.0
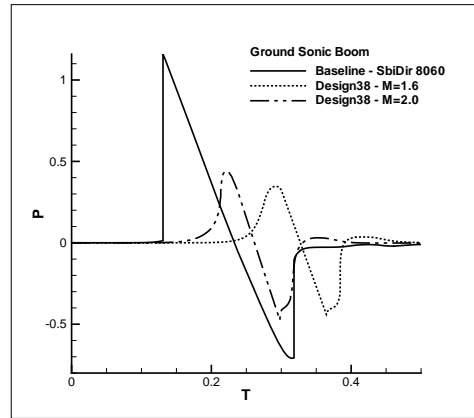
Figure 19: Computed pressure signature on the ground at AoA=2 for the baseline, Design 38 at M=1.6 and Design 38 at M=2.0
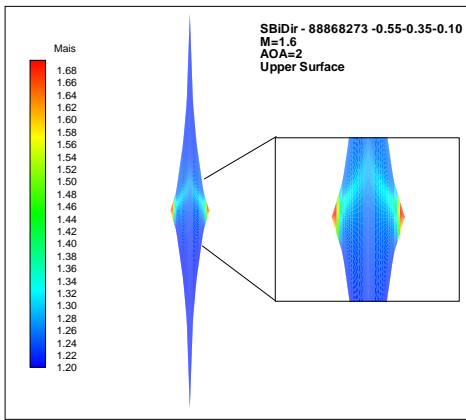
Figure 20: Computed Mach number contours at upper surface of Design38 SbiDir-FW configuration, AoA =2, M=1.6
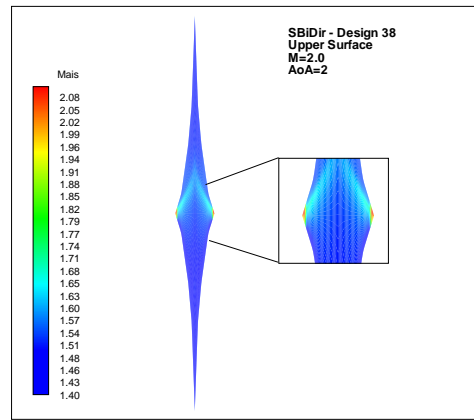
Figure 21: Computed Mach number contours at upper surface of Design38 SbiDir-FW configuration, AoA =2, M=2.0
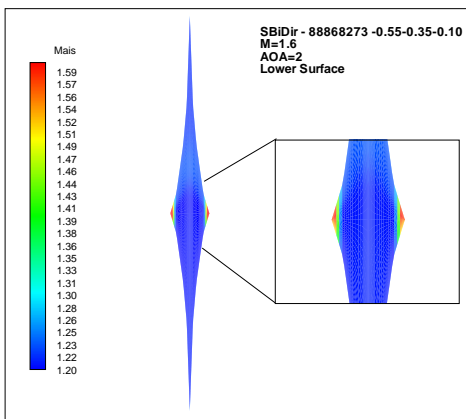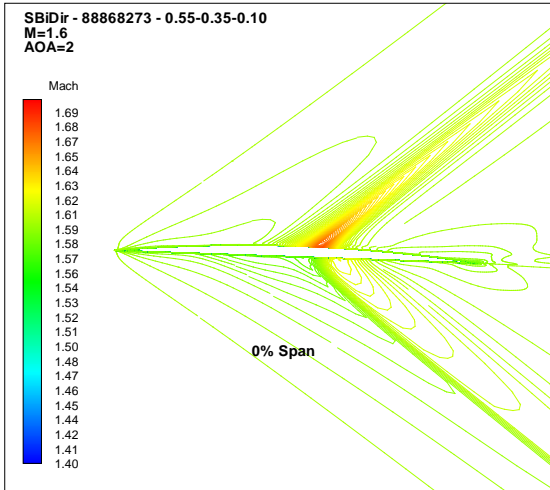

Figure 22: Computed Mach number contours on the lower surface of Design38 SbiDir-FW configuration, AoA =2, M=1.6
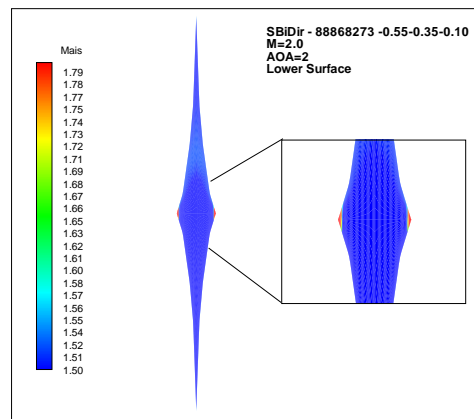
Figure 23: Computed Mach number contours at lower surface of Design38 SbiDir-FW configuration, AoA =2, M=2.0

14

Figure 24: Mach number contours at 0% span section (mid-plane), AoA=2, M=1.6
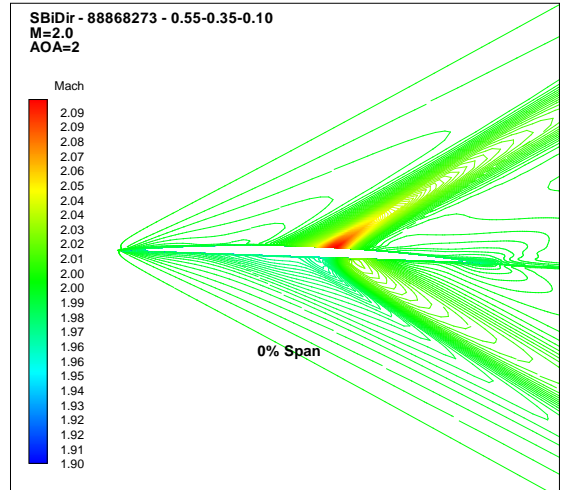
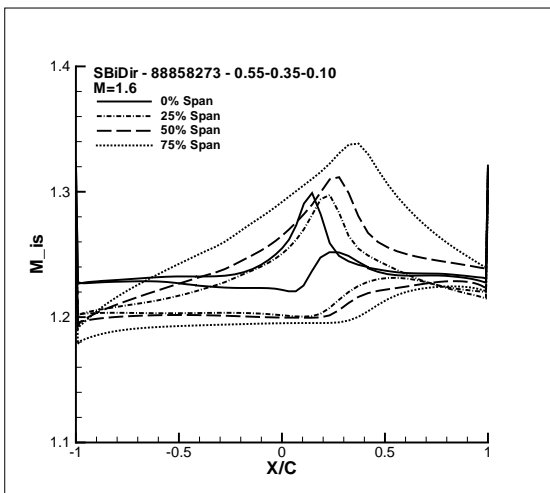Figure 25: Mach number contours at 0% span section (mid-plane), AoA=2, M=2.0

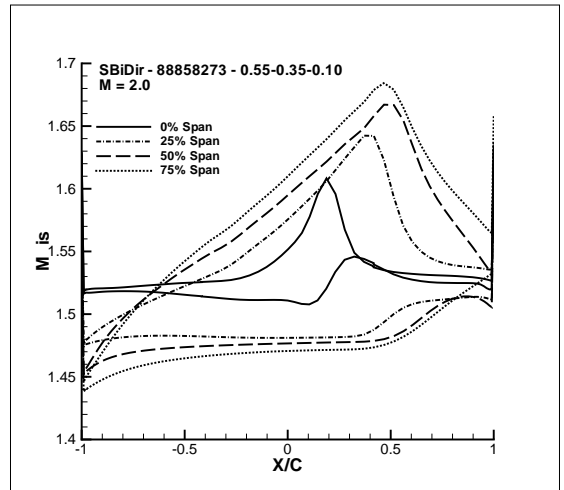Figure 26: Surface Isentropic Mach number distribution at different span section at M=1.6

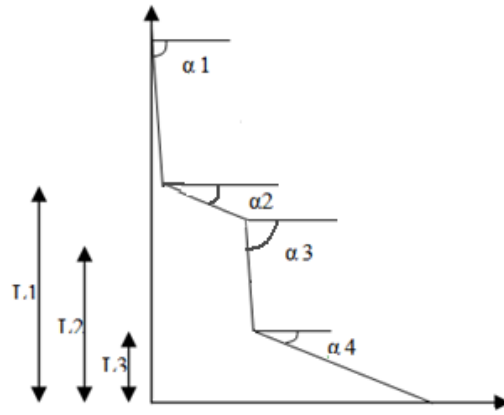Figure 27: Surface Isentropic Mach number distribution at different span section at M=2.0

15

Figure 28: Parametric definition of SbiDir-FW edge for the new design

	Cl	Cd	Cl/Cd	V	$dp_{2Lbelow}$	MoM
Variation38	0.03610	0.00231	15.58	39.9	0.00528	1
Variation47	0.02996	0.00225	13.32	31.6	0.00337	1.33

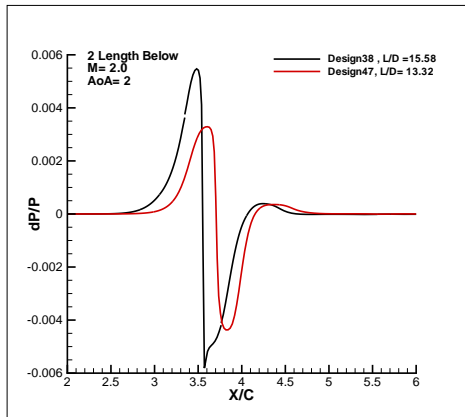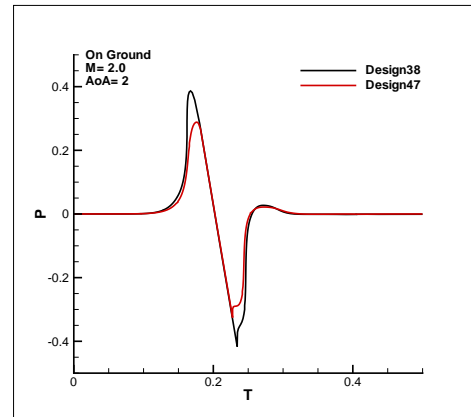Table 3: Characteristics of design 47

Figure 29: Computed overpressure 2 body length below

Figure 30: Computed overpressure on the ground